Critical mechanisms in the development of fatigue cracks in 2024-T4 aluminum

J. C. GROSSKREUTZ and G. G. SHAW

Center for Applied Research on Materials, Midwest Research Institute, Kansas City, Missouri, U.S.A.

Summary

Notched samples of 2024-T4 aluminum were partially fatigued and examined by means of optical and electron microscopy to identify the critical mechanisms for crack nucleation. Under fully reversed axial loading which led to fatigue lives of $10^5 - 10^6$ cycles, it was found that deformation in the notch began with the formation of fine slip followed by intensification of slip around inclusions. This intensified slip was accompanied by the production of small dislocation loops and dipoles. Fatigue cracks initiated at large (>1 μ) impurity inclusion clusters, and no correlation could be found between the initiation event and the formation of fine slip, concentrated slip, or dislocation dipoles and loops. All of the evidence favors the view that fatigue cracks nucleated at the interface between surface inclusions and matrix, probably by a debonding mechanism. Prior cracking of inclusions was not observed.

Introduction

The detailed micromechanisms leading to crack nucleation in pure aluminum have been well documented in recent years. Crack nucleation in commercial aluminum alloys is only poorly understood and it has not been clear whether the basic mechanisms which operate in the pure material can be invoked to describe what happens in the commercial alloys. Crack nucleation in 2024-T4 and 7075-T6 aluminum is known to occur exclusively at surface inclusions, [1, 2] and that these inclusions are hard intermetallic compounds containing primarily the impurities Fe and Si. Although the detailed micromechanisms of crack nucleation remain undefined. However whether slip bands are actually involved, and whether dislocation dipoles and cross-slip mechanisms contribute to the nucleation of an intrusion crack in the vicinity of an inclusion is not known. In this paper, these questions are subjected to close scrutiny for the case of 2024-T4 aluminum. In addition, considerable new evidence is presented for the micromechanisms of early fatigue hardening in this material.

Experimental techniques for the study of crack nucleation

High resolution microscopy of both the surface of the specimen, where a crack is most likely to nucleate, and of the near-surface material where the dislocation interactions occur which lead to crack nucleation was

used. This required that the crack nucleation site be somewhat localized so that inordinate amounts of time were not spent searching for the initial crack and for this reason, a sample in which crack nucleation was localized in a mild notch having a theoretical stress concentration factor of two was used [1, 2]. For the more specialized transmission electron microscopy of near-surface areas, a specimen in which a shallow 'dimple' at the root of the notch further localized the area of crack nucleation was used. Fatigue stressing of all samples was accomplished in a Sonntag SF-U-1 fatigue testing machine with fully reversed push-pull loading. Stress levels were chosen to give lives in the range 10^5-10^6 cycles. Normally, the net section stress was ±13,600 lb/in^2.

Routine optical examination and fax-film replication of the notch area were made at intervals during a fatigue test. For high resolution examination of the notch, special replicas were prepared for electron microscopy. Disks for transmission electron microscopy (TEM) were cut out parallel to the notch surface and included the dimple. The surface of the dimple was then coated with a layer of 'microstop', and the disk thinned for TEM by electropolishing from the opposite side [3].

Sequential events which accompany the development of fatigue cracks in 2024-T4 aluminum

Early surface deformation

Fine slip lines were observed on the surface of the notch before the appearance of fatigue cracks. These slip lines, which are illustrated in Fig. 1, occurred despite the fact that the concentrated stress at the root of the notch is only approximately one-half the yield stress of 2024-T4. Once formed, this fine slip was not observed to develop further with increased fatigue cycling.

Further insight into the manner in which this fine slip develops was obtained by TEM of the surface layer of the notch. Uncycled 2024-T4 contains many helical dislocations which are part of large dislocation loops generated during the original quench. From the TEM observations it appears that these large dislocation loops are capable of expanding near the surface under cyclic stresses which are smaller than the macroscopic yield stress. Fig. 2 illustrates the notch surface dislocation morphology in a sample that had been subjected to 240,000 cycles at a nominal stress of ±13,600 lb/in^2. Two expanding dislocation loops (shown at A and B in the figure) trail long dislocation segments which are trapped at the surface-oxide interface and which lie along the direction of the observed fine slip. Moreover, the separation of these segments is consistent with the fine slip spacing shown in Fig. 1, namely 1,000-2,000 Å. The length of these slip lines is clearly limited by interaction of the helical dislocation loops with the large elongated dispersoid

particles shown in Fig. 2. Once the existing dislocation loops have expanded and are pinned at dispersoid particles, further dislocation motion in the matrix is apparently impossible at this low stress.

Plasticity around inclusions

In addition to fine slip, much heavier concentration of slip can be found around some of the impurity inclusions, e.g. Fig. 3. The spacing of this slip is comparable to that of the fine slip and its development is apparently due to the stress concentrating effect of the inclusion. Not all inclusions are observed to have these concentrations of slip surrounding them.

Transmission electron microscopy of the deformed area around an inclusion has been accomplished; results are shown in Fig. 4. The dislocation density is much higher in this area than it was in Fig. 2. Moreover, a heavier concentration of dislocations is seen to be trapped at the oxide-surface interface along traces of the primary glide planes. Traces of a secondary slip system can also be observed in faint contrast in Fig. 4.

Nucleation of the fatigue crack

Optical examination of the fax-film replicas showed that all primary failure cracks (and indeed all secondary cracks) nucleated at surface impurity inclusions. At optical magnifications, no concentrated slip could be seen in association with these early cracks. Fig. 5 illustrates an early crack, only 10 μ long, for which extensive electron replicas were obtained as the crack developed. It should be noted that this crack has nucleated at an inclusion cluster. These clusters are a rather common site for crack nucleation. All of the observations reported here were made on samples which were electropolished prior to cycling. To test whether preferential chemical attack at the inclusions was a factor in crack initiation, identical observations were performed on mechanically polished samples. Cracks were observed to nucleate at inclusions in the same manner and after equivalent numbers of cycles. An electron surface replica taken at a somewhat later stage in the development of this crack is shown in Fig. 6; the inset shows the optical photograph at this later stage of development. Careful examination of the replica does not dislose any concentrated slip in association with the failure crack origin.

Although no other high quality electron replicas of a crack nucleation site were obtained, the general results of the investigation showed no correlation between crack nucleation and concentrated slip lines at inclusions. Careful examination of Figs. 2 and 4 and many more micrographs of similar nature has failed to reveal zones of precipitate reversion or overaging which might give rise to regions susceptible to crack nucleation. In addition, attempts to find cracked inclusions, in both uncycled and fatigued specimens were unsuccessful.

Finally, longitudinal sections were made through the nucleating inclusion shown in Figs. 5 and 6 to see whether near-surface defects were contributing to the nucleation of the crack. Fig. 7 is an optical micrograph of a section taken within $\pm 1\,\mu$ of the point indicated by the arrow in Fig. 6. This photograph shows clearly the multiplicity of inclusions which make up the cluster responsible for crack nucleation. Although polishing marks obscure the exact point of origin of the crack in this photograph, subsequent etching (which destroyed much of the inclusion detail) showed the crack to originate at the interface between the matrix and a surface inclusion (arrow, Fig. 7).

Early crack growth

Information concerning the deformation which accompanies early crack growth was obtained by transmission electron microscopy in the vicinity of the crack. This rather difficult experimental observation was achieved by starting with a dimpled specimen which contained a small crack, and electrothinning such that the final perforation occurred close enough to the crack to allow electron transmission. Fig. 8 (a) is a low magnification TEM photograph of a crack which was examined in this manner. The nucleating inclusion, part of which has dropped out during the electropolishing, is at the upper right-hand corner of the photograph. Fig. 8 (b) illustrates the dislocation configuration and metallurgical structure within $1\,\mu$ of the actual crack. The dislocation density is quite high and consists of a continuous tangled mass of dislocations with some small prismatic loops and dipoles visible. No evidence of concentrated slip or metallurgical reversion or overaging is observed. We are, in fact, observing here the evidence for a plastic zone in the immediate vicinity of the micro-crack.

Discussion of the observations

Many of the events which occur during fatigue of 2024 are not actively involved in the crack nucleation mechanism. The development of fine slip and of concentrated slip at inclusions are clearly among these noncritical events. While it would have been satisfying to see a parallel with the slip band crack initiation which occurs in fatigue of pure aluminum, such is not the case. Nor do the dislocation dipoles and loops in the vicinity of inclusions appear to play a direct role in crack initiation as they must in pure aluminum [4] where they accumulate to very high densities in slip bands prior to cracking.

We begin identification of the critical events for crack initiation by calling attention to a little-appreciated metallurgical feature of commercial 2024 which we feel plays a major role in suppressing the early formation of cracks. The so-called dispersoid particles are observed as

large, noncoherent particles in the transmission micrographs (e.g., Fig. 2) and are usually elongated in the rolling direction. These particles are complex, intermetallic compounds containing aluminum, manganese, magnesium, iron and silicon. In a high purity Al-0·6% Mn alloy they can be identified as Al_6Mn. In the T3 and T4 conditions, these dispersoid particles effectively limit the slip distance in 2024 to approximately $0{\cdot}5$-$1\,\mu$*. By limiting the slip distance, these particles also prevent the early development of concentrated zones of slip in 2024 which could be potential crack nucleation sites. Even in the vicinity of inclusions where the stress concentration is high, concentrated slip never builds up to the point necessary for continued crack growth.

Obviously the most critical features for crack nucleation in this alloy are impurity surface inclusions, and the events which occur at the matrix-inclusion interface. Although not observed directly, interface debonding would appear to be the most likely mechanism for crack initiation. The inclusions themselves are not observed to crack. Whether tiny interfacial cracks are introduced during fabrication of the alloy or whether they develop during cycling is not clear. The fact that inclusion clusters are the usual sites of crack nucleation is reasonable in either case. The stress concentration around an inclusion can be enhanced by the existence of a near neighbor.

The size of the nucleating inclusion or cluster is also important; we observe the larger ones ($>1\,\mu$) to be the most effective. The dependence of fatigue strength on inclusion size has been extensively documented in the case of steels [6, 7]. In all cases the fatigue strength was inversely proportional to the inclusion size, and inclusions at the surface were much more detrimental than subsurface inclusions. It appears from our experiments that a similar relationship holds for 2024-T4. It has already been demonstrated [8] that reduction of the Fe-Si impurity content to less than 0·1% in the 7000 series of aluminum alloys results in a significant improvement in fatigue strength. Experiments on an 'inclusion-free' 2024 alloy have begun and it is hoped to report on these in a subsequent paper.

Conclusions

Crack nucleation in commercial 2024-T4 aluminum is a highly localized event which occurs at the interface between a surface impurity inclusion (usually part of a cluster) and the alloy matrix. Interfacial debonding

* Because they are unaffected by the solution heat treatment, these particles also prevent the formation of extended quench bands in the commercial alloy. Such bands can provide regions of extended solute depletion during subsequent precipitation hardening which in turn act as localized regions of plastic instability during fatigue (5).

Fig. 3. Concentrated slip around surface inclusion after 4×10^5 cycles at ± 13,600 psi. (Same sample as Fig. 1.)

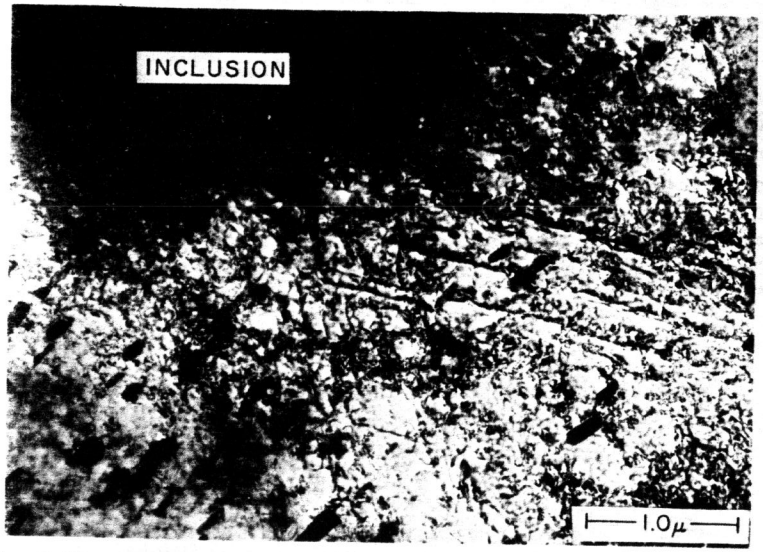

Fig. 4. Transmission electron micrograph of surface area around an inclusion. Concentrated slip traces are visible as well as many small dislocation loops. 3×10^5 cycles at ± 9,200 psi. (Dimpled specimen.)

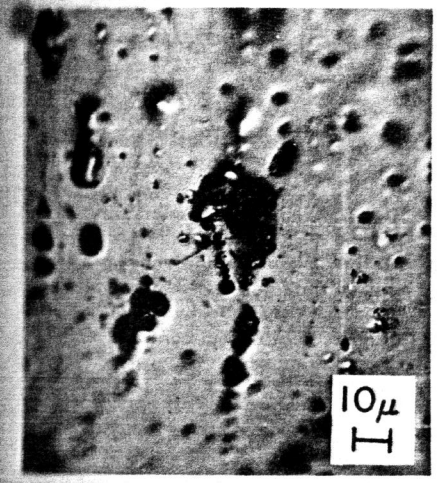

Fig. 5. Optical micrograph of early crack nucleating at inclusion. 4×10^5 cycles at ± 13,600 psi.

Fig. 7. Optical micrograph of longitudinal section through nucleation point shown in Fig. 6. Polishing scratches partially obscure point of crack nucleation indicated by arrow.

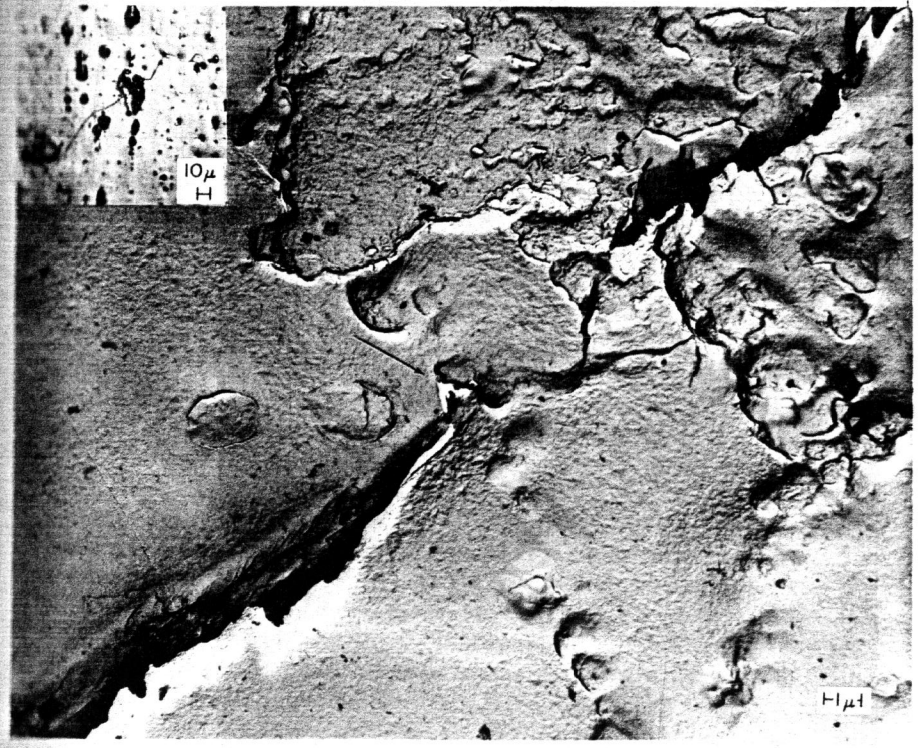

Fig. 6. High resolution replica of crack and nucleating inclusion. Arrow denotes approximate point of nucleation. Inset is optical micrograph of the crack. (Same as Fig. 5 except at 9×10^5 cycles.)

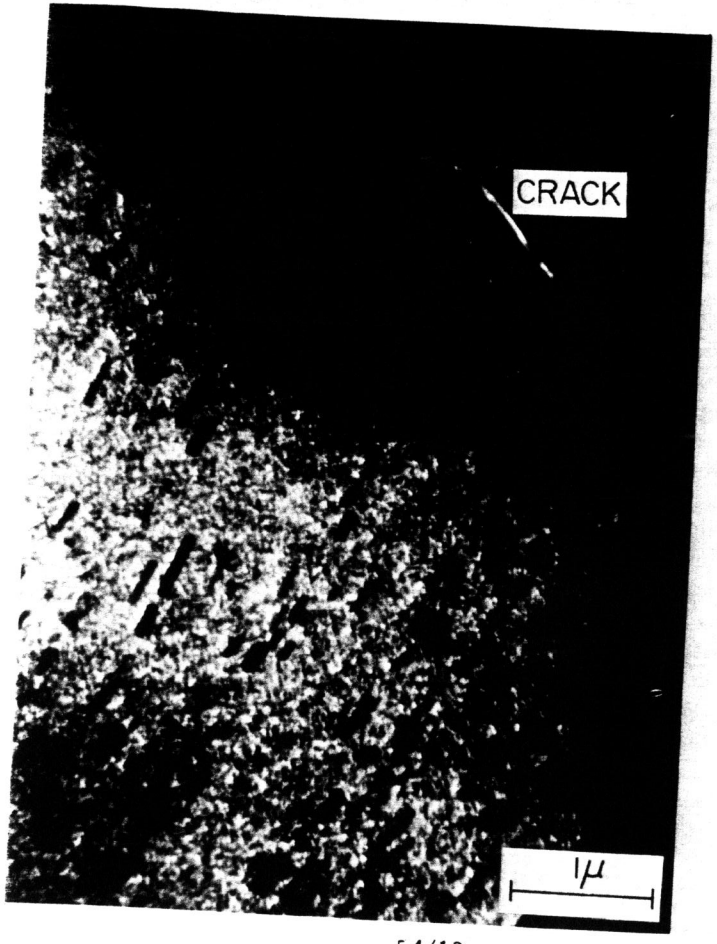

Fig. 8. Transmission electron micrograph of early microcracks: (a) Low magnification showing entire crack and nucleating inclusion; and (b) High magnification with dislocations in contrast. Crack as shown.